

Nanoscale

Accepted Manuscript



This is an *Accepted Manuscript*, which has been through the Royal Society of Chemistry peer review process and has been accepted for publication.

Accepted Manuscripts are published online shortly after acceptance, before technical editing, formatting and proof reading. Using this free service, authors can make their results available to the community, in citable form, before we publish the edited article. We will replace this *Accepted Manuscript* with the edited and formatted *Advance Article* as soon as it is available.

You can find more information about *Accepted Manuscripts* in the [Information for Authors](#).

Please note that technical editing may introduce minor changes to the text and/or graphics, which may alter content. The journal's standard [Terms & Conditions](#) and the [Ethical guidelines](#) still apply. In no event shall the Royal Society of Chemistry be held responsible for any errors or omissions in this *Accepted Manuscript* or any consequences arising from the use of any information it contains.

What are the Active Carbon Species during Graphene Chemical Vapor Deposition Growth?

Cite this: DOI: 10.1039/x0xx00000x

Haibo Shu^{ab}, Xiao-Ming Tao^a, and Feng Ding^{*a}

Received 00th January 2014,
Accepted 00th January 2014

DOI: 10.1039/x0xx00000x

www.rsc.org/

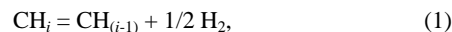
The dissociation of carbon feedstock is a crucial step for understanding the mechanism of graphene chemical vapor deposition (CVD) growth. Using first-principles calculations, we perform a comprehensive theoretical study for the population of various active carbon species, including carbon monomer and various radicals, CH_{*i*} (*i* = 1, 2, 3, 4), on four representative transition-metal surfaces, Cu(111), Ni(111), Ir(111) and Rh(111), under different experimental conditions. On the Cu surface, which is less active, the population of CH and C monomer at subsurface are found very high and thus are the most important precursors for the graphene CVD growth. On the Ni surface, which is more active than Cu, C monomers at the subsurface dominate the graphene CVD growth under most experimental conditions. Differently, on the active Ir and Rh surfaces, C monomers on the surfaces are found very stable and thus are the main precursors for graphene growth. This study shows that the mechanism of graphene CVD growth depends on the activity of catalyst surfaces and the detailed graphene growth process at atomic level can be controlled by varying the temperature or partial pressure of hydrogen.

1. Introduction

Graphene, a single-atom thickness of graphite with the *sp*² bonded honeycomb lattice, has outstanding properties and numerous potential applications, in particular as the replacement of Si in future electronics.¹⁻³ Among the known methods of graphene production, chemical vapor deposition (CVD) growth on transition-metal (TM) surfaces is known as the most promising technique for the mass production of large area, high quality graphene. In recent years, a large number of experimental studies have been devoted to the exploration of the optimum condition of graphene CVD growth. Numerous TMs, such as Cu,^{4,5} Ni,⁶ Ir,⁷ Pd,⁸ Pt,⁹ Rh,¹⁰ Ru,¹¹ etc., and their alloys¹² were found appropriate as the catalysts for graphene CVD synthesis. The mechanism of graphene growth on these catalyst surfaces have been extensively studied recently¹³⁻²⁷ but our knowledge on the mechanism at atomic level is still very limited.

In spite of these great experimental achievements, deep and comprehensive understanding on the mechanism of graphene CVD growth has not been achieved, which is known as one of the main obstacles for the further improvement of the experimental design to achieve the final goal of graphene synthesis—the wafer sized single crystalline graphene with very high quality. To achieve the optimum condition for desired graphene growth, the selection of catalyst is one of key issues. Previously, it has been noticed that the C solubility in TMs is a key factor for graphene growth. For example, catalysts like Ni, Co and Fe have very high carbon solubility and thus the growth of graphene on the TMs is a consequence of the continuous C atoms precipitated from the bulk.²⁸ In contrast, Cu has extremely low carbon solubility and thus the growth of graphene is a self-limited process, where the diffusion of C species on the Cu surface plays a crucial role.²⁹ Differently, the graphene formation on active catalyst surfaces, such as Ir, Rh and Ru, is initiated by high supersaturated C monomers on them and then dominated by the attachment of carbon clusters during growth.^{30,31} Hence, how the growth of graphene depends on the type of catalyst is a crucial issue for the comprehensive understanding on the graphene CVD growth.

In most experiments of graphene CVD growth, hydrocarbon gases are used as the carbon feedstock, and the most used one is CH₄. The decomposition of CH₄ at high temperature could lead to the formation of carbon atoms or radicals such as CH_{*i*} (*i* = 1, 2, 3) through the reaction of



either in vacuum or on the TM surfaces.³² Recently, Zhang et al.¹⁸ reported an inspiring theoretical study and showed that the dominating C species that attached to the edge of graphene during growth on Cu(111) surface might not be C monomer but the radicals such as CH_{*i*} (*i* = 1, 2, 3). As H₂ appeared on the right side of the reaction formula (1), certainly the partial pressure of H₂ in the carrier gas is important in the control the dominating carbon species for graphene CVD growth and thus might greatly affect the growth behaviour of graphene as evidenced in many experiments.³³⁻³⁶ And certainly, the activity of the catalyst would also affect the stabilities of the decomposed carbon species, CH_{*i*} (*i* = 0, 1, 2, 3), and their populations on the surfaces. As shown in previous studies, the activity of the most used catalysts follows the order of Ru ~ Rh ~ Ir > Co ~ Ni > Cu > Au ~ Ag.²²⁻²⁴ On an active catalyst surface, the radicals interact strongly with the catalyst surface and therefore are very stable.

In this article, we report a comprehensive theoretical study of the energetics, kinetics, and populations of various carbon species CH_{*i*} (*i* = 0, 1, 2, 3, 4) on four representative transition-metal surfaces (Cu(111), Ni(111), Ir(111) and Rh(111)) during the graphene CVD growth. Our results indicate that the active C species on these metal surfaces strongly depends on the metal-C interaction and the growth condition, which is responsible for the different nucleation and growth behaviours of graphene.

2. Computational Details

All calculations are performed with the density-functional theory (DFT) approach as implemented by the Vienna *ab initio* Simulation Package (VASP).^{37,38} The exchange-correlation energy is treated in the Perdew-Burke-Ernzerhof (PBE) version of the generalized-

gradient approximation (GGA) functional.^{39,40} In order to accurately describe the van der Waals interactions (vdWs) between CH₄ molecule and TM surfaces, the PBE functional with the vdWs correction (DFT-D2)⁴¹ has also been used. The energy cutoff of the plane-wave expansion is set to 400 eV. The Monkhorst-Pack k-point mesh of 4×4×1 is found to provide sufficient accuracy in the Brillouin zone integration. All structures were optimized by conjugate gradient method until the forces acting on each atom are less than 0.01 eV/Å. The climbing image nudged elastic band (CI-NEB) method⁴² was used to determine the energy barriers of various kinetic processes.

All four metal surfaces (Cu(111), Ni(111), Ir(111), and Rh(111)) are modelled by using slab geometry with four metal atomic layers in which the bottom-layer atoms are fixed at their respective bulk positions. The unit cells of the slabs are 8.85 Å × 10.22 Å, 8.63 Å × 9.97 Å, 9.40 Å × 10.86 Å, and 9.32 Å × 10.76 Å for Cu(111), Ni(111), Ir(111), and Rh(111) surfaces, respectively. The metal surfaces with in-plane periodicity are separated by ~12 Å vacuum layer to prohibit the interactions of neighboring surface slabs. For the geometry optimization, all atoms except for the fixed bottom-

layer atoms have been fully relaxed and then various CH_i (*i* = 0, 1, 2, 3, 4) species are put on metal substrate surface for further optimization.

3. Results and Discussion

We firstly focus on the relative binding strength of various CH_i (*i* = 0, 1, 2, 3) species on TM surfaces. The binding energies E_b which is defined as:

$$E_b = E_M + E_{\text{CH}_i} - E_T, \quad (2)$$

where E_T , E_M , and E_{CH_i} are the energies of a given structure, metal substrate, and CH_i species, respectively. During the graphene CVD growth, the strong TM-C binding is needed for a CH_i specie to be adsorbed on the TM surfaces and be involved in the graphene nucleation and growth. In order to locate the optimum adsorption sites, both the surface and subsurface adsorption have been considered. As shown in Fig. 1a, the considered sites for the surface adsorption include the top (T), fcc hollow (F), hcp hollow (H) and bridge (B) sites, and one octahedral site (O) and two tetrahedral sites (TE1 and TE2) are considered for the subsurface adsorption.

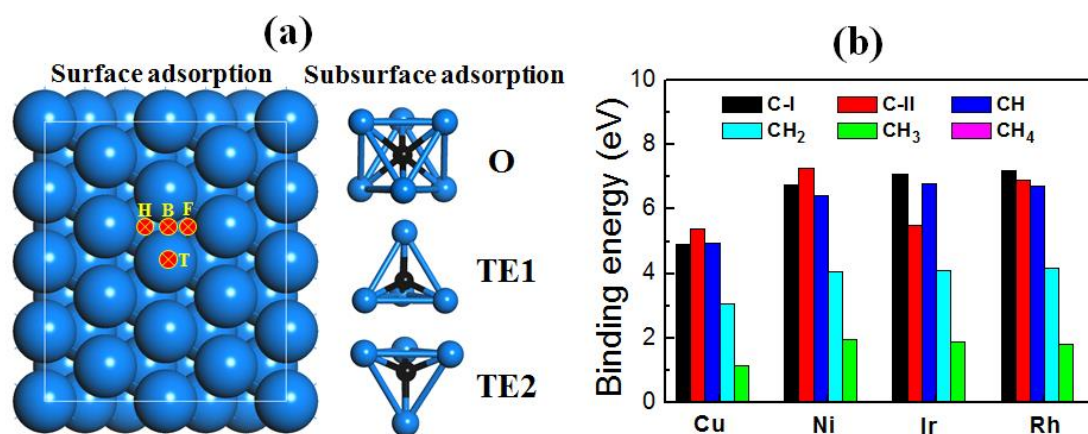


Fig. 1 (a) Adsorption sites and (b) binding energies of various CH_i species on four representative transition-metal surfaces (Cu, Ni, Ir, and Rh). Surface adsorption sites include the top (T), hcp hollow (H), fcc hollow (F), and bridge (B) sites, and the subsurface adsorption sites include one octahedral site (O) and two tetrahedral sites (TE1 and TE2), respectively. C-I and C-II represent the carbon atom on metal surface and subsurface, respectively.

The calculated binding energies of CH_i (*i* = 0, 1, 2, 3, 4) on these sites are summarized in Table 1 and the binding energies at their optimum adsorption sites are shown in Fig. 1b. For both Cu(111) and Ni(111) surfaces, C monomer at the octahedral site (O) of the subsurface (named C-II) has the largest binding energies of 5.40 and 7.27 eV, respectively. These calculated energies are in good agreement with that reported in literature.⁴³ While the C-II at the tetrahedral sites (TE1 and TE2) of the subsurface is not stable and it will migrate to another site during structural optimization. For example, the C-II at TE1 moves to the O site and the C-II at the TE2 moves to the H site. On Ir(111) and Rh(111) surfaces, the C monomer on surface (C-I) is more stable than that at the subsurface. The binding energies of C-I on Ir(111) and Rh(111) surfaces are 7.08 and 7.21 eV, respectively, which are 1.57 and 0.31 eV higher than the C-II that at the subsurface, respectively.

On each of the explored TM surface, increasing H component in CH_i always leads to weaker binding as expected. The binding energies of a CH₄ molecule on all metal surfaces are nearly zero (~0-0.05 eV) which implies that the very weak interaction between CH₄ and metal substrates is not sufficient to bind the molecule on the metal surface and therefore the CH₄ molecules should not be counted as an active C specie in graphene growth. It's necessary to mention that the GGA-PBE method can't treat the weak vdWs interaction between a CH₄ molecule and a TM surface well. To provide more

accurate data, the binding energies of CH_i (*i* = 0-4) on these metal surfaces have been calculated by the DFT method with the vdWs correction (DFT-D2 method) and the results are listed in Table S1 in the ESI†. The binding energies of a CH₄ molecule on the four TM surfaces calculated by DFT-D2 method are ~0.2 eV larger than those calculated by the GGA-PBE method. Moreover, we also found that the binding energies of other active species, CH_i (*i* = 0, 1, 2, 3), are method dependent. Nevertheless, the CH_i-metal interactions (*i* = 0, 1, 2, 3) are mainly contributed by the chemical bonding and thus the results from GGA-PBE should be valid. As shown in Fig. 1b, the binding energies of all other CH_i species (*i* = 0-3) are greater than 1.0 eV and thus they can be held on the catalyst surfaces for a sufficient long time and be involved in the graphene nucleation and growth. In another words, they are all active for graphene growth on these catalyst surfaces.

It's interesting that the binding energy increment of CH_i species on metal surfaces with the H components is almost linear (see Fig. S1†). The scale relation between CH_i binding energies and the H component agrees well with previous theoretical report by Nørskov *et al.*⁴⁴. The binding energy of CH_i (*i* = 1, 2, 3, 4) on these catalyst can be fitted by

$$E_b(i) = E_0 - ai, \quad (3)$$

Table 1. Binding energy E_b (in eV), diffusion barrier E_D (in eV), and diffusion path of various C precursors on Cu, Ni, Ir and Rh surfaces. C-I and C-II represent the carbon monomer on metal surface and subsurface, respectively. The character T, F, H, and B denote the top, fcc, hcp, and bridge adsorption sites on metal surfaces, and O, TE1 and TE2 denote octahedral and tetrahedral adsorption sites on metal subsurface, respectively. N/A represent that the carbon species at the site are not stable after structural optimizations and they will move to other adsorption sites.

On Cu(111)						
Surface	E_b (eV)				E_D (eV)	Diffusion path
	T	F	H	B		
C-I	N/A	4.90	4.87	4.86	0.25	H→F→H
CH	N/A	4.96	4.90	N/A	0.30	H→F→H
CH ₂	N/A	3.05	3.01	N/A	0.33	H→F→H
CH ₃	0.97	1.14	1.06	1.05	0.31	H→F→H
CH ₄	0.05				-	-
Subsurface	O	TE1	TE2			
C1-II	5.39	N/A	N/A		0.86	O→F
On Ni(111)						
Surface	T	F	H	B	E_D (eV)	Diffusion
C-I	N/A	6.70	6.76	N/A	0.29	H→F→H
CH	N/A	6.42	6.40	N/A	0.30	H→F→H
CH ₂	N/A	4.06	4.01	N/A	0.16	H→F→H
CH ₃	1.63	1.98	1.95	1.78	0.15	H→F→H
CH ₄	0.06				-	-
Site	O	TE1	TE2		0.78	O→O
C1-II	7.27	N/A	N/A		1.06	O→F
On Ir(111)						
Surface	T	F	H	B	E_D (eV)	Diffusion
C-I	5.67	6.87	7.08	N/A	1.35	H→F→H
CH	4.94	6.78	6.78	N/A	1.18	H→F→H
CH ₂	3.46	4.10	4.08	4.08	0.88	H→F→H
CH ₃	1.87	1.44	1.52	N/A	0.64	F→T→F
CH ₄	0.04				-	-
Subsurface	O	TE1	TE2			
C1-II	5.51	5.48	N/A		1.18	O→F
On Rh(111)						
Surface	T	F	H	B	E_D (eV)	Diffusion
C-I	5.20	7.03	7.21	N/A	0.82	H→F→H
CH	N/A	6.68	6.72	N/A	0.74	H→F→H
CH ₂	3.30	4.16	4.13	4.07	0.37	H→F→H
CH ₃	1.77	1.83	1.81	1.75	0.34	H→F→H
CH ₄	0.03				-	-
Subsurface	O	TE1	TE2			
C1-II	6.90	6.50	N/A		1.08	O→F

Table 2 The fitted parameters E_0 (in eV) and α for the binding energies of CH_i species on Cu, Ni, Ir and Rh surfaces.

Parameters	Cu	Ni	Ir	Rh
E_0 (eV)	5.82	7.73	7.77	7.84
α (eV)	1.45	1.89	1.90	1.93

where E_0 and α depends on the type of catalysts and can be viewed as the indicators for the activeness of the catalyst surface. The fitted numbers of E_0 and α are shown in Table 2. It can be clearly seen that the binding strength of these carbon species on these metal surfaces follows the order of $\text{Cu} < \text{Ni} \sim \text{Ir} \sim \text{Rh}$. The difference of CH_i -metal binding strength can be understood by the d -band model.⁴⁴ In this model, the interaction between a CH_i and a metal surface strongly depends on the width and energy of metal's d states which play an important role in adjusting the p - d hybridization of adsorbent and metal surface. The relatively weak binding strength of CH_i on Cu(111) surface arises from the difference of d -band energies between Cu and other metal surfaces. Similar results about the activity of TM surfaces have also been demonstrated in previous studies.²⁴

Among the four active carbon species, the binding energies of CH_3 on these catalyst surfaces are in the range of 1.14 - 1.87 eV. The

thermal dynamic life time of a species on the catalyst surface can be estimated by

$$\tau = \tau_0 \exp(E_b/k_B T), \quad (4)$$

where $\tau_0 = h/k_B T$, h and k_B are the Plank and Boltzmann constants, respectively. Hence, the lifetime of a CH_3 at a typical temperature of graphene CVD growth ($T = 1000$ - 1300 K) ranges from 10^{-8} to 10^{-4} s, which is very short for the species to diffuse a longer distance on the catalyst surfaces. In contrast, all other species (C, CH and CH_2) has much stronger binding energy ($E_b > 3.0$ eV) and their lifetime on the catalyst surfaces reaches 10^3 s or longer. So, we conclude that C monomer, CH and CH_2 should be the three crucial species for graphene CVD growth.

We next investigate the relative stabilities and population of these active species CH_i ($i = 0, 1, 2, 3$) on these TM surfaces. Because hydrogen is often involved in graphene CVD growth, the relative Gibbs free energy (ΔG_f) of a specie should be defined as⁴⁵⁻⁴⁷:

$$\Delta G_f = E_T - E_M + \Delta F_{\text{vib}} - n_C \mu_C - n_H \mu_H \quad (5)$$

where $n_C = 1$ and $n_H = i$ are the number of C and H atoms in CH_i , respectively. ΔF_{vib} is the vibrational contribution to Gibbs free energy of CH_i species, μ_C and μ_H are carbon and hydrogen chemical potentials respectively and they depend on the growth temperature and partial pressure of H_2 and CH_4 . The computational details for the determination of relative Gibbs free energy, ΔF_{vib} , and atomic chemical potentials have been presented in ESI†.

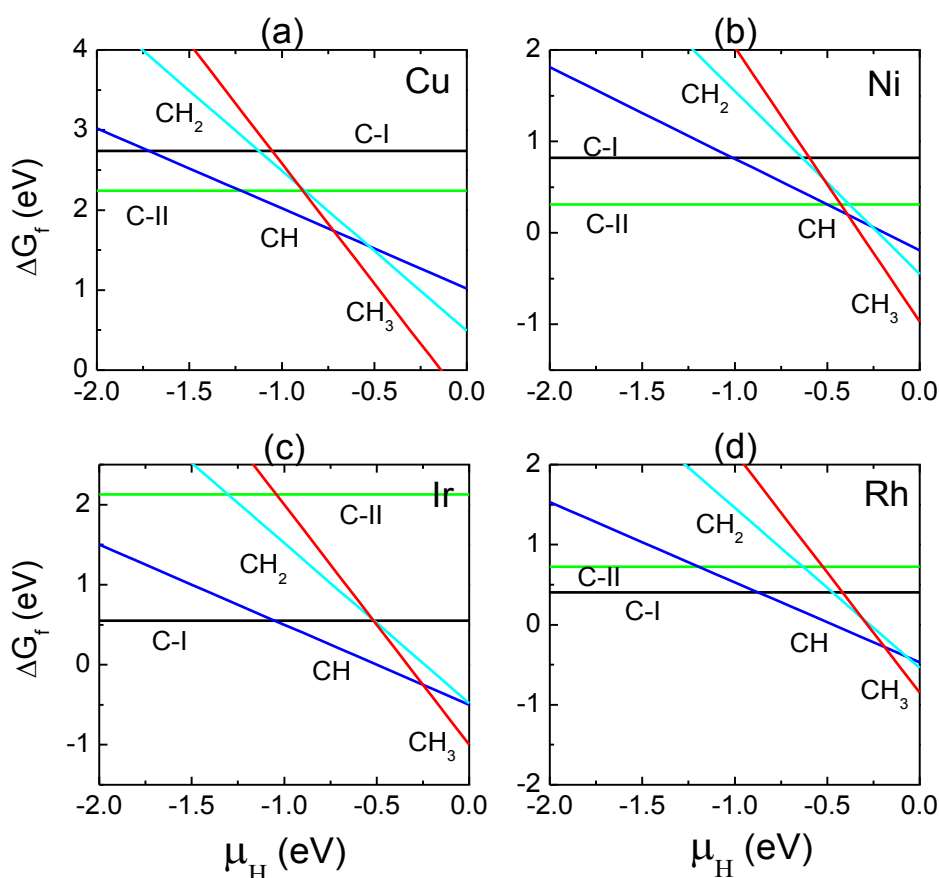


Fig. 2 Relative Gibbs free energy ΔG_f of various CH_i species ($i = 0$ -3) on (a) Cu(111), (b) Ni(111), (c) Ir(111), and (d) Rh(111) surfaces as a function of μ_H . C-I and C-II represent the carbon monomer on metal surface and subsurface, respectively.

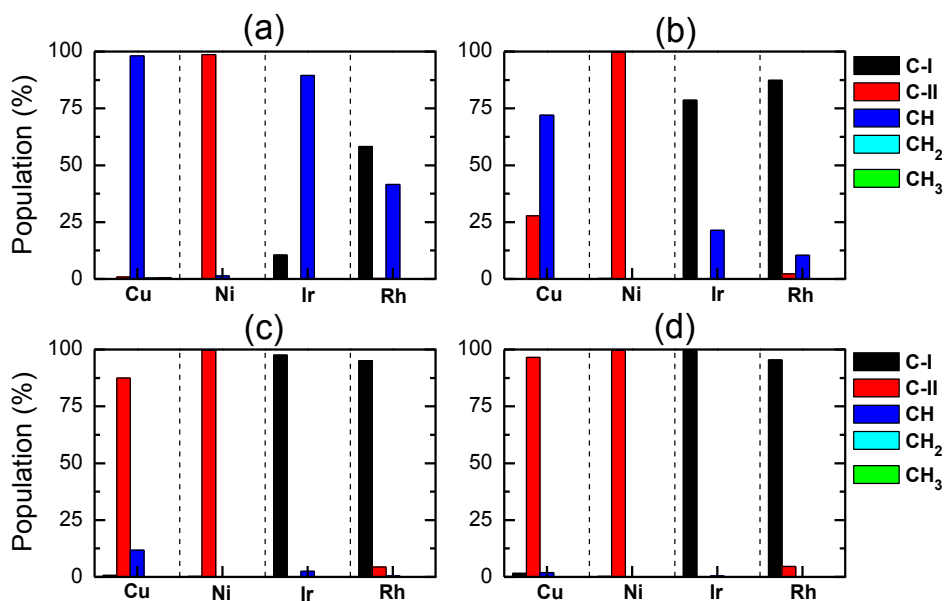


Fig. 3 Relative population of various CH_i species ($i = 0, 1, 2, 3$) on Cu(111), Ni(111), Ir(111), and Rh(111) surfaces for the temperature T at (a) 800 K, (b) 1000 K, (c) 1200 K, and (d) 1400 K, respectively; where the H_2 pressure is set to 10^{-2} mbar and μ_{C} is set to the energy of C atom in graphene. C-I and C-II represent the carbon atom on metal surface and subsurface, respectively.

Fig. 2 shows that the relative Gibbs free energies of species CH_i ($i = 0, 1, 2, 3$) on the four TM surfaces as a function of μ_{H} , and μ_{C} is set to the energy of C atom in graphene (-9.233 eV/atom). It is found that the stability of CH_i highly depends on μ_{H} . On the Cu(111) surface (see Fig. 2a), the most stable CH_i species in the regime of $\mu_{\text{H}} > -0.72$ eV is CH_3 , then becomes the CH in the regime of $\mu_{\text{H}} \in [-1.24$ eV, -0.72 eV], and then C atom at the subsurface (C-II) for $\mu_{\text{H}} < -1.24$ eV. CH_2 never be the dominate species because its binding energy lies between those of CH and CH_3 . The result indicates that high dehydrogenation level of feedstock is preferred with the decrease of μ_{H} . Similar trend has been observed on Ni(111) surface (see Fig. 2b), but the regime for the CH to be dominate is very narrow and the C-II is the dominating specie when $\mu_{\text{H}} < -0.53$ eV. The stability of CH_i ($i = 0, 1, 2, 3$) on Ir(111) and Rh(111) surfaces are very similar (see Fig. 1(c) and Fig. 1(d)). With the reduction of H chemical potential, the most stable CH_i species changes from CH_3 to CH, and then to C monomer on surface (C-I).

Most graphene CVD growth occurs at a high temperature range of $800 \text{ K} < T < 1400 \text{ K}$, at which the μ_{H} ranged from -1.6 to -0.6 eV, depending on the partial pressure of H_2 (Fig. S2†). Certainly such a large μ_{H} could significantly affect the population of each carbon species. To explicitly show the abundance of each carbon specie, the relative population (P_i) of the CH_i ($i = 0, 1, 2, 3$), which is defined as:

$$P_x = \exp(-\Delta G_f^x / kT) / \sum_x \exp(-\Delta G_f^x / kT), \quad (6)$$

on the four TM surfaces and at $T = 800, 1000, 1200$ and 1400 K , respectively, and with a H_2 partial pressure of 10^{-2} mbar are shown in Fig. 3a-3d.

It can be clearly seen that the dominating CH_i specie strongly depends on both temperature and the type of TM surface. At 800 K, the dominating C species on Cu(111) surface are CH and C-II has higher population on Ni(111). While, on the Ir(111) and Rh(111) surfaces, the CH and C-I are the dominating C species. This results are in consistent with those experimental observations^{48,49}, in which

nucleation density of graphene on TM surfaces is low at lower temperature due to the incomplete dehydrogenation of feedstock.

Increasing temperature leads to the reduction of μ_{H} and large population of highly dehydrogenated species. At 1000 K (see Fig. 3b), on Cu(111) surface, the surface species are mainly CH and part of C-II. On Ni(111), the populations of C-II is dominating, which implies that nearly all the feedstock completely dehydrogenated. While on Ir(111) and Rh(111), CH and C-I are dominating but the C-I has higher population. At 1200 K (see Fig. 3c), C-II indicates higher population than CH on Cu surface and fully dehydrogenated feedstock is dominating for all other three TM surfaces. At even higher temperature, $T = 1400 \text{ K}$ (Fig. 3d), the fully dehydrogenated C-I or C-II becomes the dominating carbon species on all four TM surfaces.

From above analysis, we can conclude that, under the condition of most CVD experiments, C monomer and the CH are two competitive species on Cu, Ir and Rh surfaces. They are more active than CH_2 and CH_3 and thus the growth of graphene should be mainly due to the attachment of C monomer and CH onto the edge of graphene domains. In particular for Cu surface, the CH is very active carbon specie and the combination of CH specie may induce the formation of C_2H_2 , namely, $\text{CH} + \text{CH} \rightarrow \text{C}_2\text{H}_2$. Previous theoretical study¹⁸ also found the highly stable C_2H_2 on Cu(111) surface even at the high temperature of CVD growth (e.g., $T \sim 1300 \text{ K}$). Combining two CH species into a C_2H_2 is an exothermic process with the energy release of 1.94 eV and an activation energy barrier of 0.3 eV. Therefore, the C_2H_2 can also be an important intermediate for the nucleation and growth of graphene on Cu surface. On the Ni surface, the role of CH can be ignored due to the very low population and activity. For graphene growth at high temperature (e.g., $T \sim 1300 \text{ K}$), which is known required for the fast growth of high quality graphene on all catalyst surfaces, the C monomer is the only dominating C species. This result partially explained the requirement of high temperature for high quality graphene CVD growth.

In addition to the temperature, H_2 and CH_4 partial pressures (P_{H_2} and P_{CH_4}) also play a crucial role in the graphene CVD growth. As

shown in Fig. S2†, P_{H_2} affects μ_H greatly. Choosing a typical growth temperature, $T = 1200$ K, Fig. 4 presents the populations of various CH_i species on four TM surfaces as a function of P_{H_2} . As expected from above discussion, only two species, CH and C monomer, have significant populations in the large P_{H_2} range from 10^{-4} to 10^2 mbar, which covers most experimental conditions. Increasing P_{H_2} always leads to larger population of CH. On Cu(111) surface (Fig. 4a), increasing P_{H_2} range from 10^{-4} to 10^2 mbar leads to a rise of the CH population from 1% to 75% and the deduction of the population of C monomer from 96% to 15%. Such a great change in the population of active carbon species must leads to a significant change in growth behavior. As evidenced experimentally, the graphene grown on Cu surface can be tuned to be rounded, hexagonal and branched shapes by simply tuning the partial pressure of H_2 .^{5,50} On the Ni(111)

substrate (Fig. 4b), the populations of CH_i ($i = 0, 1, 2, 3$) species is very different from those on Cu(111) surface. It can be found that carbon monomer at the subsurface is the only dominating species in the whole P_{H_2} range. It means that the dehydrogenation of feedstock on Ni is very complete and C monomers tend to diffusion into Ni substrate. This has been evidenced as the formation of surface carbide phase (Ni_3C phase) on Ni.⁶ On Ir(111) and Rh(111) surfaces (see Fig. 4c and Fig. 4d), it can be observed that the main active C species are the surface C monomer on the surface (C-I) for the low H_2 pressure, but the population of CH gradually increases with the increasing H_2 pressure. Considering the higher activity of C monomer than CH, the dominating specie for graphene growth on Ir(111) and Rh(111) should be C monomer as well. Therefore, increasing H_2 pressure should not affect the growth behavior notably.

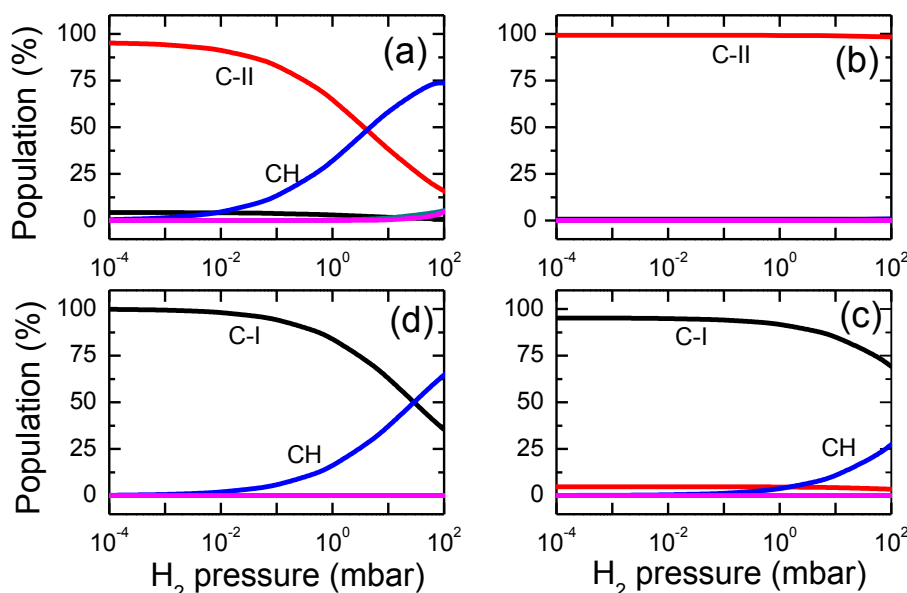


Fig. 4 Population of various CH_i species ($i = 0-3$) on (a) Cu(111), (b) Ni(111), (c) Ir(111), and Rh(111) surfaces as a function of H_2 pressure, the growth temperature T is set to 1200 K. C-I and C-II represent the carbon atom on metal surface and subsurface, respectively.

During the graphene CVD growth, the ratio of P_{CH_4} and P_{H_2} , χ , is another important factor for adjusting the carbon chemical potential (μ_C) and Gibbs free energy of CH_i species on TM surface. Hence, the population of CH_i may be changed by adjusting the χ . To highlight the role of $\chi = P_{CH_4}/P_{H_2}$, we have considered four different χ , namely, $\chi = 100, 1, 0.01$, and 0.0001 . The computational detail for the dependence of μ_C on χ has been presented in ESI†. As shown in Fig. S3†, μ_C increases with the increase of χ for a given H_2 pressure but the increment of μ_C between two χ ratios is still same in the allowed range of H_2 pressure. For example, μ_C at $\chi = 0.0001$ is still 0.95 eV lower than that at $\chi = 1$ in all allowed range of H_2 pressure. Therefore, adjusting χ value leads to the change of Gibbs free energy. However, according to the definition of CH_i population (see Eq.(6)), the population of CH_i species will not be changed when relative Gibbs free energies of all CH_i species were changed in same fold.

Beyond the thermodynamics, the kinetics is another important issue of graphene CVD growth. The kinetics of CH_4 dissociation on TM surfaces is a basic step for the nucleation and growth of graphene. The dehydrogenation from a CH_4 molecule to a C atom needs to overcome a series of activity barriers (E_A). Thus, the magnitude of activity energy barriers in the reaction process of dehydrogenation will also affect the population of CH_i species on TM surfaces. Recently, Zhang *et al.*¹⁸ reported the decomposition of CH_4 molecule on Cu surface by using the first-principle calculations.

They found that the E_A values in the range of 0.9~2.0 eV, in which the reaction step of $CH \rightarrow C$ has the largest activity barrier. It implies that CH should have a higher population than C monomer on Cu surface. In contrast, the dehydrogenation of CH_4 on Ni, Ir, and Rh surfaces has relatively lower activity energy barriers due to high surface activity. For example, the E_b values are only 0.2~1.3 eV and the calculated forward rate constants at 900 °C are beyond 2.6×10^8 per second in all reaction steps of CH_4 dissociation on Ni surface.⁵¹ Therefore, the kinetics of CH_4 dissociation on active TM surfaces should have less influences on the population of CH_i species during the graphene CVD growth.

As evidenced experimentally, the diffusion limited growth behavior have been observed in graphene growth on various catalyst surfaces, which implies that the diffusion of the active carbon species on the catalyst surface is another key issue that determines the mechanism of graphene growth. Here the diffusion barriers of CH_i ($i = 0, 1, 2, 3$) on the four TM surfaces is explored by the climbing nudged energy band (c-NEB) method,⁴² incorporated in the VASP package. Several possible diffusion pathways, including of surface diffusion, subsurface diffusion and the diffusion from the subsurface to surface, are considered for each species as shown in Table 1 and Fig. S4†. Except for CH_3 on Ir(111), the optimum diffusion part for CH_i ($i = 1, 2, 3$) is between two hollow sites (or $H \rightarrow F \rightarrow H$ as listed in Table 1). The subsurface diffusion of C

monomer via the hopping between two octahedral interstitial sites, namely $O \rightarrow O$, was found the lowest energy path. In addition, we also considered the diffusion of C monomers from the subsurface to surface and the pathway is noted as $O \rightarrow F$. The calculated lowest diffusion barriers of various CH_i species on four TM surfaces have been shown in Table 1 and Fig. S4†. On the Cu(111) surface, C-II and CH are two key species under most conditions of graphene growth. The surface diffusion barrier of CH on Cu(111) surface is only 0.30 eV and the barrier of C-II is 0.63 eV. On the Ni(111) substrate, the C-II is the dominating specie under all the conditions of graphene growth. The diffusion of C-II in subsurface is 0.78 eV. Although the diffusion barriers of other CH_i ($i = 1, 2, 3$) species are very low (< 0.3 eV) on Ni surface, they have little effect on graphene growth due to their very small populations.

Owing to the low population of C atoms on Ir(111) and Rh(111) surfaces, the required C atoms during the graphene nucleation and growth are mainly supplied by the surface diffusion. The diffusion barriers of C/CH on Rh(111) and Ir(111) surfaces are 0.82/0.72 and 1.35/1.18 eV, respectively. Among all the explored catalyst surfaces, the diffusion barriers on Ir(111) surface are the largest, especially for C monomer. Such a high barrier must limit the even distribution of active carbon species on the catalyst surface and thus homogeneously nucleation of many nuclei on Ir(111) surface is expected and observed experimentally.⁵²

Conclusions

In conclusion, we have performed a comprehensive study of the energetics, population, and kinetics of various potential CH_i species ($i=0, 1, 2, 3, 4$) on Cu(111), Ni(111), Ir(111), and Rh(111) surfaces during the graphene CVD growth. Different from the conventional viewpoint, the CH species with a higher population and low diffusion barrier should be responsible for the slow growth rate of graphene on Cu surface due to H-passivated edge by the incorporation of CH. The C atom in subsurface is found to be the active C species on Ni(111) substrate, which agrees well with the experimental observations that C adatoms prefer to diffuse into the Ni substrate under the growth condition. On Ir(111) and Rh(111) surfaces, the main active C species are surface C adatom, which implies that graphene grows via the attachment of supersaturated C atoms on these metal surfaces. Our results indicate that these active C species in the CVD growth strongly depend on the activity of the catalyst surface and the growth condition (temperature, H_2 pressure, etc.), which provides a pathway to control the graphene growth by the selection of the catalysts and other parameters.

Acknowledgements

This work was supported in part by Hong Kong RGC-GRF grants (B-Q35N and B-Q26K), NSFC grant (21273189 and 11404309). Computational resources from the Shanghai and Tianjin Supercomputer Centers are acknowledged.

Notes and references

^a Institute of Textiles and Clothing, Hong Kong Polytechnic University, Hong Kong, China. E-mail: Feng.Ding@polyu.edu.hk

^b College of Optical and Electronic Technology, China Jiliang University, Hangzhou, China

† Comparison of binding energies of various C precursors on four TM surfaces by using DFT-D2 and GGA-PBE methods; Binding energies of CH_i species on TM surfaces as a function of H number in the CH_i species;

Computational details for the determination of relative Gibbs free energies, ΔF_{vib} , and atomic chemical potentials; Diffusion paths and barriers of CH_i species on TM surfaces. See DOI: 10.1039/b000000x/

- 1 A. K. Geim and K. S. Novoselov, *Nat. Mater.*, 2007, **6**, 183-191.
- 2 J. U. Park, S. W. Nam, M. S. Lee and C. M. Lieber, *Nat. Mater.*, 2012, **11**, 120-125.
- 3 A. Dunuev, D. V. Kosynkin, A. Sinitskii, A. Slesarev, Z. Sun and J. M. Tour, *Science*, 2011, **311**, 1168-1172.
- 4 X. S. Li, C. W. Magnuson, A. Venugopal, R. M. Tromp, J. B. Hannon, E. M. Vogel, L. Colombo and R. S. Ruoff, *J. Am. Chem. Soc.* 2011, **133**, 2816-2819.
- 5 D. Geng, B. Wu, Y. Guo, L. Huang, Y. Xue, J. Chen, G. Yu, L. Jiang, W. Hu and Y. Liu, *Proc. Nat. Acad. Sci. U. S. A.* 2012, **109**, 7992-7996.
- 6 J. Lahiri, T. Miller, L. Adamska, I. I. Oleynik and M. Batzill, *Nano Lett.* 2011, **11**, 518-522.
- 7 A. T. N'Diaye, S. Bleikamp, P. J. Feibelman and T. Michely, *Phys. Rev. Lett.* 2006, **97**, 215501.
- 8 S.-Y. Kwon, C. V. Ciobanu, V. Petrova, V. B. Shenoy, J. Bareño, V. Gambin, I. Petrov and S. Kodambaka, *Nano Lett.* 2009, **9**, 3985-3990.
- 9 L. Gao, W. C. Ren, H. L. Xu, L. Jin, Z. X. Wang, T. Ma, L. P. Ma, Z. Y. Zhang, Q. Fu, L. M. Peng, X. H. Bao and H. M. Cheng, *Nat. Comm.* 2011, **3**, 699.
- 10 M. Liu, Y. Gao, Y. Zhang, Y. Zhang, D. Ma, Q. Ji, T. Gao, Y. Chen and Z. F. Liu, *Small* **2013**, **9**, 1360-1366.
- 11 Y. Que, W. Xiao, X. Fei, H. Chen, L. Huang, S. X. Du and H.-J. Gao, *Appl. Phys. Lett.* 2014, **104**, 093110.
- 12 X. Liu, L. Fu, N. Liu, T. Gao, Y. F. Zhang, L. Liao and Z. F. Liu, *J. Phys. Chem. C*, 2011, **115**, 11976-11982.
- 13 H. Chen, W. G. Zhu and Z. Y. Zhang, *Phys. Rev. Lett.* 2010, **104**, 18610.
- 14 W. Chen, H. Chen, H. P. Lan, P. Cui, T. P. Schulze, W. G. Zhu and Z. Y. Zhang, *Phys. Rev. Lett.* 2012, **109**, 265507.
- 15 V. I. Artyukhov, Y. Y. Liu and B. I. Yakobson, *Proc. Nat. Acad. Sci. U. S. A.*, 2012, **109**, 15136-15140.
- 16 D. J. Cheng, G. Barcaro, J. C. Charlier, M. Hou and A. Fortunelli, *J. Phys. Chem. C*, 2011, **115**, 10537-10543.
- 17 Y. Wang, A. J. Page, Y. Nishimoto, H. J. Qian, K. Morokuma and S. Irle, *J. Am. Chem. Soc.*, 2011, **133**, 18837-18842.
- 18 W. H. Zhang, P. Wu, Z. Y. Li and J. L. Yang, *J. Phys. Chem. C*, 2011, **115**, 17782-17787.
- 19 P. Wu, H. J. Jiang, W. H. Zhang, Z. Y. Li, Z. H. Hou and J. L. Yang, *J. Am. Chem. Soc.*, 2012, **134**, 6045-6051.
- 20 L. Meng, Q. Sun, J. Wang and F. Ding, *J. Phys. Chem. C*, 2012, **116**, 6097.
- 21 X. Y. Zhang, Z. W. Xu, H. Li, J. Xin and F. Ding, *J. Phys. Chem. Lett.* **2012**, **3**, 2822-2827.
- 22 L. Wang, X. Y. Zhang, H. L. W. Chan, F. Yan and F. Ding, *J. Am. Chem. Soc.*, 2013, **135**, 4476-4482.
- 23 H. B. Shu, X. S. Chen, X. M. Tao and F. Ding, *ACS Nano*, 2012, **6**, 3243-3250.
- 24 Q. H. Yuan, J. F. Gao, H. B. Shu, J. J. Zhao, X. S. Chen and F. Ding, *J. Am. Chem. Soc.*, 2012, **134**, 2970-2975.
- 25 J. F. Gao, J. Yip, J. J. Zhao, B. I. Yakobson and F. Ding, *J. Am. Chem. Soc.*, 2011, **133**, 5009-5015.
- 26 P. Wu, W. H. Zhang, Z. Y. Li and J. L. Yang, *Small*, 2014, **10**, 2136-2150.
- 27 H. B. Shu, X. S. Chen and F. Ding, *Chem. Sci.*, 2014, **5**, 4639-4645.
- 28 X. Li, W. Cai, L. Colombo and R. S. Ruoff, *Nano Lett.*, 2009, **9**, 4268-4272.
- 29 Z. Luo, Y. Lu, D. W. Singer, M. E. Berck, L. A. Somers, B. R. Goldsmith and A. T. Charlie, *Chem. Mater.* 2011, **23**, 1441-1447.
- 30 E. Loginova, N. C. Bartelt, P. J. Feibelman and K. F. McCarty, *New J. Phys.*, 2008, **10**, 093026.
- 31 A. Zangwill and D. D. Vvedensky, *Nano Lett.*, 2011, **11**, 2092-2095.
- 32 Z. C. Li, P. Wu, C. X. Wang, X. D. Fan, W. H. Zhang, X. F. Zhai, C. G. Zeng, Z. Y. Li, J. L. Yang and J. G. Hou, *ACS Nano*, 2011, **5**, 3385-3390.
- 33 X. F. Zhang, J. Ning, X. L. Li, B. Wang, L. Hao, M. H. Liang, M. H. Lin and L. J. Zhi, *Nanoscale* 2013, **5**, 8363.
- 34 I. Vlasiouk, M. Regmi, P. Fulvio, S. Dai, P. Datskos, G. Eres and S. Smirnov, *ACS Nano*, 2011, **5**, 6069-6076.

- 35 S. Bhaviripudi, X. T. Jia, M. S. Dresselhaus and J. Kong, *Nano Lett.* 2010, **10**, 4128-4133.
- 36 L. Gao, W. Ren, J. Zhao, L.-P. Ma, Z. Chen and H.-M. Cheng, *Appl. Phys. Lett.* 2010, **97**, 183109.
- 37 P. E. Blöchl, *Phys. Rev. B*, 1994, **50**, 17953-17979.
- 38 G. Kresse and J. Furthmüller, *Phys. Rev. B*, 1996, **54**, 11169-11186.
- 39 J. P. Perdew, K. Burke and M. Ernzerhof, *Phys. Rev. Lett.*, 1996, **77**, 3865-3868.
- 40 G. Kresse and D. Joubert, *Phys. Rev. B*, 1999, **59**, 1758-1775.
- 41 S. Grimme, *J. Comput. Chem.*, 2006, **27**, 1787-1799.
- 42 G. Henkelman, B. P. Uberuaga and H. Jonsson, *J. Chem. Phys.*, 2000, **113**, 9901-9904.
- 43 O. V. Yazyev and A. Pasquarello, *Phys. Rev. Lett.*, 2008, **100**, 156102.
- 44 F. Abild-Pedersen, J. Greeley, F. Studt, J. Rossmeisl, T. R. Muter, P. G. Moses, E. Skulason, T. Bligaard, and J. K. Nørkov, *Phys. Rev. Lett.*, 2007, **99**, 016105.
- 45 C. G. Van de Walle and J. Neugebauer, *Phys. Rev. Lett.*, 2002, **88**, 066103.
- 46 Y. Kangawa, T. Ito, A. Taguchi, K. Shiraishi and T. Ohachi, *Surf. Sci.*, 2001, **493**, 178-181.
- 47 K. Reuter and M. Scheffler, *Phys. Rev. B*, 2001, **65**, 035406.
- 48 R. Addou, A. Dahal, P. Sutter and M. Batzill, *Appl. Phys. Lett.*, 2012, **100**, 021601.
- 49 L. X. Liu, H. L. Zhou, R. Cheng, Y. Chen, Y.-C. Lin, Y. Q. Qu, J. W. Bai, I. A. Ivanov, G. Liu and Huang, Y. et al. *J. Mater. Chem.*, 2012, **22**, 1498-1503.
- 50 B. Wu, D. C. Geng, Y. L. Guo, L. P. Huang, Y. Z. Xue, J. Zheng, J. Chen, G. Yu, Y. Q. Liu, L. Jiang and W. P. Hu, *Adv. Mater.*, 2011, **23**, 3522-3525.
- 51 K. Li, C. Z. He, M. G. Jiao, Y. Wang and Z. J. Wu, *Carbon*, 2014, **74**, 255-265.
- 52 J. Coraux, A. T. N'Diaye, M. Engler, C. Busse, D. Wall, N. Buckanie, F.-J. M. Z. Heringdorf, R. V. Gastel, B. Poelsema and T. Michely, *New. J. Phys.*, 2009, **11**, 023006.